Research Article | Vol. 27, No. 11 | 27 May 2019 | OPTICS EXPRESS 16195
Optics EXPRESS

Omnidirectional whispering-gallery-mode lasing in GaN microdisk obtained by selective area growth on sapphire substrate

JIE'AN JIANG,[1,2,3] HOUQIANG XU,[2,3] MOHEB SHEIKHI,[2,3] LIANG LI,[2,3,4] ZHENHAI YANG,[2,5,] JASON HOO,[6] SHIPING GUO,[6] YUHENG ZENG,[2] WEI GUO,[2,*] AND JICHUN YE[2,3,7]

[1]*School of Physical Science and Technology, ShanghaiTech University, Pudong, Shanghai, 201210, China*
[2]*Ningbo Institute of Materials Technology and Engineering, Chinese Academy of Sciences, Ningbo, 315201, Zhejiang, China*
[3]*University of Chinese Academy of Sciences, Beijing, 100049, China*
[4]*School of Materials Science and Engineering, Shanghai University, Shanghai, 200444, China*
[5]*Department of Electrical and Electronic Engineering, Faculty of Science and Engineering, University of Nottingham Ningbo China, Ningbo 315100, China*
[6]*Advanced Micro-Fabrication Equipment Inc. Shanghai, 201201, China*
[7]*jichun.ye@nimte.ac.cn*
[*]*guowei@nimte.ac.cn*

Abstract: The optical properties of hexagonal GaN microdisk arrays grown on sapphire substrates by selective area growth (SAG) technique were investigated both experimentally and theoretically. Whispering-gallery-mode (WGM) lasing is observed from various directions of the GaN pyramids collected at room temperature, with the dominant lasing mode being Transverse-Electric (TE) polarized. A relaxation of compressive strain in the lateral overgrown region of the GaN microdisk is illustrated by photoluminescence (PL) mapping and Raman spectroscopy. A strong correlation between the crystalline quality and lasing behavior of the GaN microdisks was also demonstrated.

1. Introduction

Edge-emitting ultraviolet laser diodes (UV-LD) have drawn intensive interests recently due to wide applications in medical diagnostics, chemical sensing, water purification *etc* [1,2]. Many efforts have been made in the past decade in the development of UV-LD [3–5], but there are still many challenges that impede the progress towards higher efficiency of the devices, for example, high dislocation densities in the active region and difficulties to achieve smooth and parallel Fabry-Perot (F-P) cavities to provide enough gain over losses during light amplification. These critical obstacles can be surmounted by introducing microdisk whispering gallery mode (WGM) lasers, which have advantages such as wider wavelength coverage, lower optical loss and lasing threshold, and better high-speed modulation characteristics compared to that for F-P lasers. WGM lasers have been mostly fabricated on the Si substrate due to strong light reflection at the GaN/Si interface, and easier formation of overhang pivoted nitride microdisk on Si posts by wet chemical etching [6]. It is also compatible with the large-scale IC fabrication process and can be implemented into the optical interconnections. However, Si-based WGM lasers suffer from low crystalline quality, affecting both internal quantum efficiency (IQE) and threshold current of the LD due to the large lattice and thermal mismatch between III-nitride and Si substrate [7]. In addition, since reactive ion etching (RIE) is usually applied in the formation of the III-nitride WGM microdisk, severe light scattering and large optical losses are inevitable as mask erosion during RIE results in rough sidewalls and degradation of circularity of the GaN microdisks

#364098 https://doi.org/10.1364/OE.27.016195
Journal © 2019 Received 2 Apr 2019; revised 4 May 2019; accepted 4 May 2019; published 22 May 2019

Optics EXPRESS

[7]. Compared to GaN microdisk fabricated by RIE [8], microdisks obtained by bottom-up growth method have advantages, such as higher crystalline quality, naturally formed crystallographic planes acting as side-reflecting mirrors, and consequently improved lasing characteristic [9].

As a typical bottom-up growth technique, selective area growth (SAG) of III-nitride rods or hexagonal disks on sapphire substrate has been reported before by numerous researchers [10]. It was demonstrated that SAG technique can effectively reduce the defect density since a large portion of the microdisk is grown laterally on SiO_2 mask, blocking threading dislocations stemming from the underlying GaN or sapphire template. It was also reported that SAG can also reduce piezoelectric polarization and improve the efficiency of electron-hole recombination through growing nonpolar sidewall surfaces [11]. Collective lasing behavior and capabilities in tuning the direction of emitted light were obtained by growing InGaN-based nanorods in the form of two-dimensional periodic array [12]. Nevertheless, the correlations between structural quality, strain state and lasing behavior of the GaN microdisks have seldom been studied before.

In this work, GaN microdisks in periodic arrays were grown on sapphire substrate by SAG technique. WGM lasing characteristic from the hexagonal resonators was discussed as a function of both collection angle and light polarization degree. Spatially-resolved photoluminescence (PL) and cathodoluminescence (CL) properties of the GaN microdisks were also investigated, illustrating that the overgrown region of the GaN microdisk with good crystalline quality greatly helps in the process of light amplification and omnidirectional lasing.

2. Experimental details

Hexagonal GaN microdisk arrays were grown on patterned SiO_2 on GaN/sapphire template using an AMEC Prismo HiT3^{TM} MOCVD reactor in N_2 ambient. Trimethylgallium (TMG)/triethylgallium (TEG) and ammonia (NH_3) were used as precursors of Ga and N, respectively. The total pressure is 200 torr and V/III is 100. Firstly, 5 μm thick GaN epitaxial layer was grown on 2 inch sapphire substrate. Then, 150 nm thick SiO_2 was deposited on GaN epitaxial layer by electron beam evaporation technique. Circular microholes with diameter of 2 μm and 20 μm were fabricated on SiO_2 by conventional photolithography followed by RIE. After patterning of SiO_2, the templates were subjected to sonication in acetone, methanol and DI water for 5 min, respectively. Then, the templates were reloaded into MOCVD chamber for re-growth of GaN microdisks. Surface morphologies of the GaN microdisk arrays were characterized by a Hitachi s4800 Scan Electron Microscope (SEM) and Veeco Dimension 3100 V AFM. Steady-state room temperature PL analysis and Raman analysis were carried out using a Renishaw inVia Reflex spectrometer system with a 325 nm He-Cd laser and 532 nm Nd-YAG laser as excitation sources, respectively. In the spatially-resolved PL measurement, the output power of the incident beam was set as 25 mW with a scanned area about 30 × 30 μm^2. Luminescence was collected using the objective lens of 50X from the same side and analyzed by the built-in spectrometer. The spontaneous and stimulated emissions of the GaN microdisks were investigated using an Ar-F (193 nm) excimer laser at various excitation power densities, and both the edge and surface emissions were collected by a Horiba iHR550 spectrometer dispersed by a 1200 lines/mm grating to a cooled charged-coupled device (CCD) under room temperature (RT). In addition, Glan-Taylor polarizers were used for polarization dependent spectral analysis. RT and low temperature (LT) CL characterizations were performed utilizing a FEI Quanta FEG 250 in combination with a Gatan MonoCL setup.

3. Results and discussions

Top-view SEM images revealing the surface morphologies of the GaN microdisk arrays are shown in Fig. 1(a) and (b). SiO_2 microhole arrays with diameter/periodicity of 2/20 μm and

Optics EXPRESS

20/40 μm were utilized during SAG pattern fabrication, and the outlines of the SiO_2 microholes are denoted by the dashed red circles in Fig. 1(a-b). Hexagonal microdisks are bounded by (10-1-1) planes, and the lengths of the side facets of the hexagonal GaN are 5 and 14 μm, respectively. For simplicity reason, they are denoted as 5 and 14 μm microdisk. It was observed that similar lateral expansion of approximately 4 μm were illustrated for both 5 μm and 14 μm microdisks, indicating that lateral growth rate is the same in spite of the dimension of GaN microdisk, and the SAG is lateral diffusion controlled [13]. The surface morphologies of 5 μm and 14 μm microdisk are dramatically different. Rough surface is observed on top of the 5 μm microdisk, whereas the surface of the 14 μm microdisk is atomically flat with corresponding root mean square (RMS) roughness of only 1.13 nm. The growth mechanism of SAG GaN is illustrated in Fig. 2(a)-(d). During the early stage of the growth process, flat and smooth top surface is achieved by step-flow growth mode of GaN inside the SiO_2 holes. Subsequently 3D growth becomes dominant, forming rough top surface, until GaN gradually fills SiO_2 microholes and crystal coalesce. Finally, as crystal grains coalesce into each other, semi-polar (10-1-1) planes start to become the terminating sidewalls due to their lower surface energies [14]. Clearly, surface morphology of the 5 μm microdisk can be represented by the growth condition shown in Fig. 2(c), whereas that of the 14 μm microdisk is denoted as Fig. 2(b).

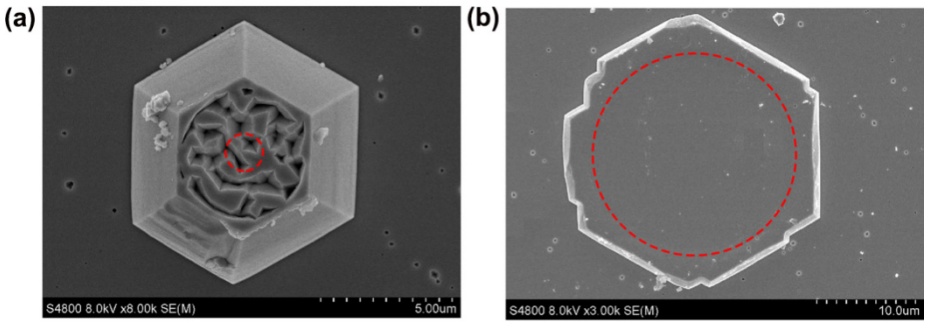

Fig. 1. Top-view SEM images of Single GaN microdisk with side length of 5 μm (a) and 14 μm (b). The outlines of the underlying SiO_2 microholes are marked with the dashed red.

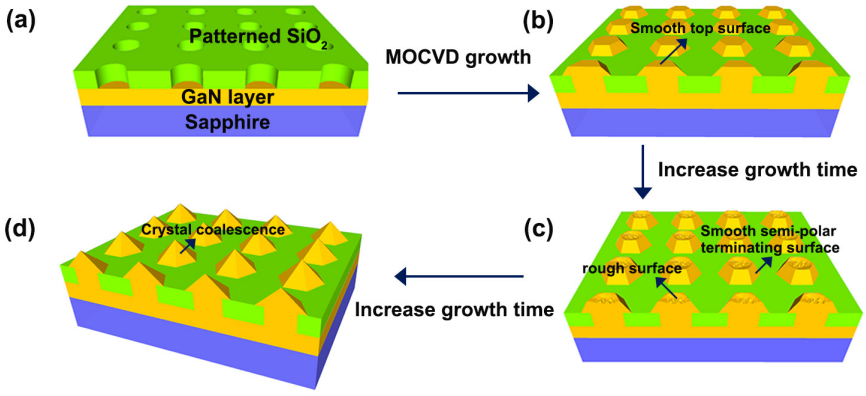

Fig. 2. Schematic process flow in fabricating GaN hexagonal microdisk arrays on the surface of patterned SiO_2/GaN/sapphire: As-fabricated patterned SiO_2 circular microholes (a); Growth front evolution of the GaN hexagonal microdisk (b)-(d).

The schematic setup of the RT PL measurement is shown in Fig. 3(a) [15]. The sample is put on an X-Y stage with lateral resolution of 10 nm. For power-dependent PL measurement, laser excitation is fixed along the surface normal of the GaN microdisk, with the excitation

Optics EXPRESS

area being approximately 1 × 1 mm^2, covering a large number of GaN microdisks. The influence of the pumping power on the edge emission spectra of the 14 μm GaN microdisk arrays is illustrated as an example in Fig. 3(b). At low pumping powers, GaN microdisk arrays exhibit broad spontaneous emission peaks. Several optical modes are identified with mode spacing approximately 2 nm. A clear distribution of cavity modes from M1 to M9 locating at 368.4, 370.6, 372.3, 373.9, 376.5, 379.4, 382.5, 386.1 and 389.8 nm are clearly shown. As excitation power increases, PL intensity dramatically increases. At excitation energy above 2 MW/cm^2, an obvious resonant peak centered at 372.3 nm emerged, becoming the dominant mode [16]. However, which mode become dominant depends on various factors including optical path, microdisk geometry, and collection direction. In this work, the excitation area is 1 × 1 mm^2, which is much larger than the dimension of the microdisk itself. Therefore, the work reported here represents a collective lasing phenomenon, and the precise control of the exact lasing mode seems to be difficult due to competing lasing behaviors from various GaN microdisks.

It is worth noting that, below the lasing threshold, two modes are located at 372.3 and 373.9 nm independently. However, the two modes merge into one sharp peak, and the relative intensity of the 373.9 nm mode is increasing against the one at 372.3 nm, which could be distinguished in Fig. 3(c). Therefore, a gradual redshift of 0.3 nm is observed as a result of the above two competing modes and the FWHM of 372.3 nm mode above the lasing threshold cannot be further reduced. The influence of the pumping power on the integrated intensity and full-width-half-maximum (FWHM) of the 372.3 nm mode is shown in Fig. 3(d). Super-linear increase of the peak intensity together with dramatic reduction of the FWHM below 2 nm indicate light amplification in the 14 μm GaN hexagonal microdisks [17] owing to decent light confinement properties inside the overgrown GaN microdisk, even it was grown on sapphire substrate. The lasing threshold (E_{th}) is determined to be 2.43 MW/cm^2 based on the evolution of PL intensities and spectral width of the dominant resonant peak. WGM lasing in 5 μm GaN microdisk was also observed. The lasing threshold of 5 μm GaN microdisk is approximately 3 MW/cm^2, which is similar to that of 14 μm GaN microdisk. The size dependence on the lasing characteristic is not observed in this study.

Many efforts have been made in the past decade in the development of GaN microdisk WGM laser on Si. Choi *et al*. reported that stimulated emission of arrays of pivoted GaN microdisks of 20 μm diameter fabricated on GaN/Si template by a combination of dry and wet etching was achieved [18]. Baek et al. described methods to grow GaN microdisks of 5 μm diameter on amorphous silicon oxide layers on Si using micropatterned graphene films as a nucleation layer, and the lasing threshold was 250 kW/cm2 [17]. In this work, GaN microdisk arrays were grown on sapphire substrate, in which case the refractive index difference is smaller compared to that of GaN/Si system. In addition, serious leakage of emission out of these structures would occur at the GaN/sapphire interfaces, leading to increased lasing thresholds. Thus, the lasing threshold of ~2.43 MW/cm^2 is within expectation, even though further structure optimization is needed in order to achieve lower threshold and larger output power.

Typical far-field patterns recorded on a screen made of printer paper placed approximately 1 cm away from the edge of the 14 μm GaN microdisk arrays is shown in Fig. 4(a)-(d) for pumping powers below and above lasing threshold E_{th} at RT. Below E_{th}, there is no obvious light spot since spontaneous emission is emitted randomly in all directions, and the output power is relatively weak. Above E_{th} a strong spot pattern appears on the screen, and the intensity becomes stronger as increasing pumping power, clearly indicating the occurrence of stimulated emission.

Optics EXPRESS

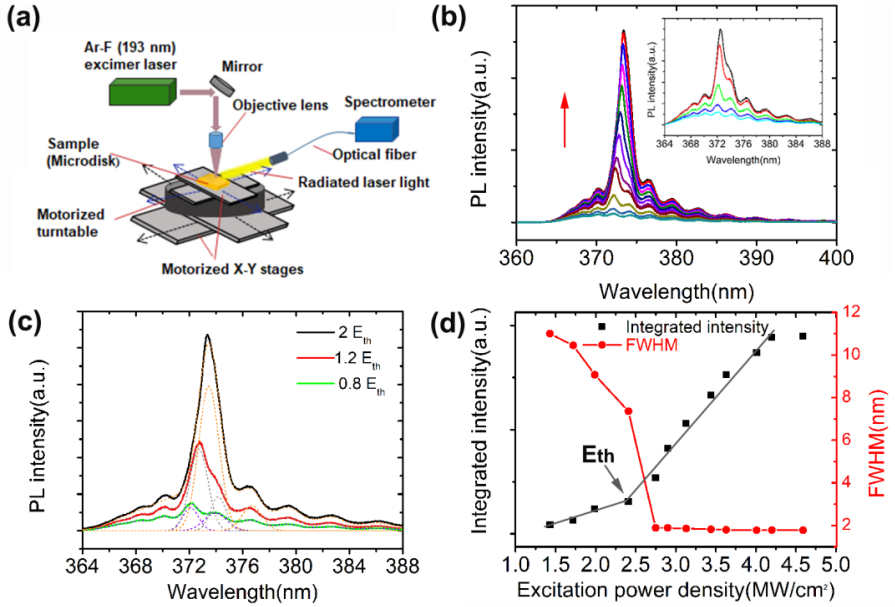

Fig. 3. Schematic setup of μ-PL measurement system (a); RT-PL spectra of 14 μm microdisk arrays under different pumping powers (b). Inset image shows a zoom-in view of the emissions below lasing threshold; The zoom-in view of the evolution of two modes located at 372.3 and 373.9 nm, respectively, at pumping power below lasing threshold and above lasing threshold (c); The influence of pumping power on the integrated intensity and FWHM of the edge emission of 14 μm microdisk arrays (d).

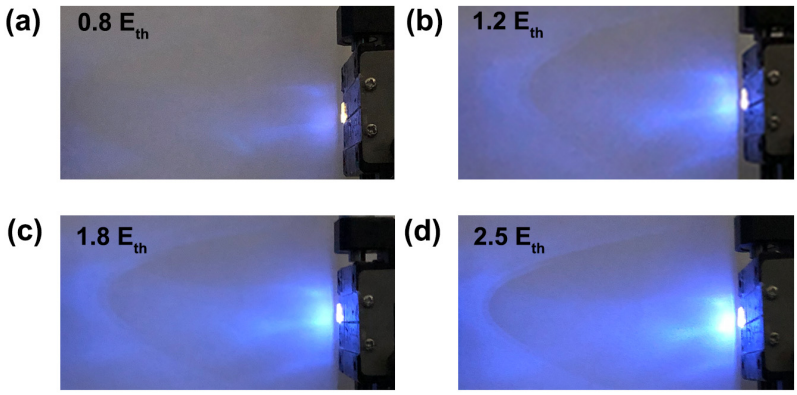

Fig. 4. Far-field patterns observed below (a) and above threshold (b)-(d) by setting a sheet of white copying paper in front of the edge of 14 μm GaN microdisk arrays under optical pumping (the pulse width was 5 ns, and the repetition rate 50 Hz) at room temperature, and a blue luminescence formed when the near-UV light illuminated the white copying paper.

Angular-resolved PL characterization was performed to understand the directional behavior of the WGM lasing. The laser is incident on the sample 30° away from the surface normal. The angle between the optical fiber and the surface normal of the GaN microdisk ranges from 0° to 90° as shown in Fig. 5(a). Optical fiber is aligned either along ***m*** or ***a*** direction of the GaN microdisk. It is found that lasing spectra collected from both directions are similar, but the PL spectra collected along ***a*** direction illustrate lower lasing threshold, possibly due to enhanced light-field scattering at the corners of the GaN microdisk [15]. Figure 5(b) shows the PL spectra of the 14 μm GaN microdisk arrays collected at different θ angles above lasing threshold. Both spontaneous and stimulated emissions are observed. As θ

Optics EXPRESS

increases, the intensity of the broad spontaneous emission peak of GaN microdisk below lasing threshold decreases in both ***m*** and ***a*** directions due to reduced cross-section of the emitting area, whereas the stimulated emission peak prevails relatively, indicating a dominant light amplification effect along the edges of the GaN microdisk. Lasing peaks with similar FWHM values are clearly shown for all θ angles, indicating omnidirectional reflection of the stimulated emission and various trajectories of the reflected light at the (0001) and (10-1-1) crystal planes. Moreover, the stimulated emission peak is located at the long-wavelength-side of the spontaneous emission peak, most probably due to stronger re-absorption at the high-energy parts of the spontaneous emission spectrum [19].

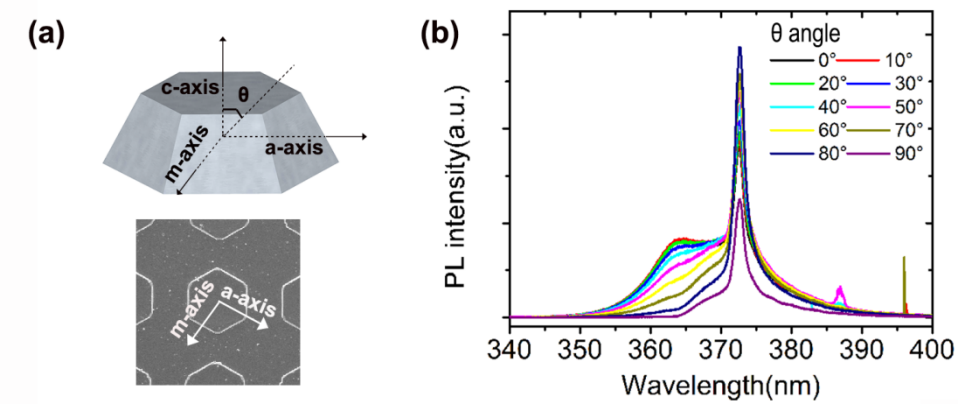

Fig. 5. Angular-resolved PL measurement in a three-dimensional illustration, together with a top-view SEM image indicating the collection direction of the optical fiber (a); PL spectra of the 14 μm microdisk arrays above lasing threshold (b).

It is mentioned above that light can travel around the sidewalls of the hexagonal microdisk with little loss by total internal reflection. Thus F-P mode lasing is less likely to occur due to absence of parallel cavity [17]. It should be noted that the clearest distinction between F-P type modes and WGM-type modes is the mode spacing [20]. For F-P cavity mode, mode spacing Δλ between adjacent peaks can be calculated by Eq. (1) [21]

$$\Delta\lambda = \frac{\lambda^2}{2\mathrm{d}\left(n - \lambda\frac{dn}{d\lambda}\right)}. \tag{1}$$

where ***n*** = 2.6 is the refractive index of GaN at lasing wavelength of 372.3 nm, ***d*** is the cavity length, ***λ*** = 372.3 nm is the lasing wavelength, $dn/d\lambda$ is –0.003 nm^{-1} at 372.3 nm, denoting the dispersion relation shown in Eq. (2) [15].

$$n^2 - 1 = 2.60 + \frac{1.75\lambda^2}{\lambda^2 - 0.256^2} + \frac{4.1\lambda^2}{\lambda^2 - 17.86^2}. \tag{2}$$

As calculated from Fig. 3(b), Δλ = 1.6 nm, resulting in ***d*** = 29 μm, which is unreasonable for F-P cavity since the thickness of our GaN microdisk is only 2.5 μm. The observed lasing characteristic is believed to be either attributed to WGM or quasi-WGM resonance depending on the optical paths inside the hexagon disk. For WGMs within the microdisk cavities, the mode spacing Δλ can be calculated by Eq. (3) [22]:

$$\Delta\lambda = \frac{\lambda^2}{2\pi \mathrm{n}_{\mathrm{eff}} R} \tag{3}$$

Optics EXPRESS

where λ, R, and neff represent the resonant wavelengths, radius of the microdisk cavity, and effective refractive index, respectively. Δλ is calculated to be 0.6 nm, which is much larger than the resolution of our spectrometer of 0.1 nm.

To further investigate the polarization property of the stimulated emission, a Glan-Taylor polarizer was put in front of the optical fiber, as it was previously reported that both transverse magnetic (TM) and transverse electric (TE) polarized emissions are involved in the WGM lasing [23]. Emission spectra are collected as a function of azimuth angle Φ, which is the rotation angle between the Glan-Taylor prism and the sample surface above the lasing threshold. The emission spectra from the 14 μm GaN microdisk arrays at various azimuth angles are shown in Fig. 6(a) and the integrated PL intensity as a function of Φ is shown in Fig. 6(b). 0° represents fully TE polarization light, and 90° is denoted as fully TM polarization light. It shows that TE mode dominates over TM mode, with 3.5 times higher in PL intensity. The dominant TE-polarized emission from the WGM lasing can be ascribed to positive (Δ_{cr} = + 38 meV) crystal-field splitting energy in the valence band of GaN, and thus transition from the conduction band to the valence band with Γ_9 symmetry [24]. The polarized emission spectra have slightly higher FWHM values of 2 nm, most probably due to the large distance between the edge of the GaN microdisk and the optical fiber due to insertion of the polarizer and consequently deviation from the lasing direction.

To further confirm TE-mode WGM lasing characteristics, the theoretical resonant wavelengths of a WGM lasing in 14 μm microdisk are calculated by Eq. (4) below using a plane wave approximation [25].

$$\frac{9}{2}\mathrm{L}\times n=\lambda[N_{TE}+\frac{3}{\pi}\arctan(n\sqrt{\frac{n^2-4}{3}})] \tag{4}$$

where $\boldsymbol{N_{TE}}$ is an integer, $\boldsymbol{\lambda}$ is the wavelength, $\boldsymbol{n}$ is the refractive index, and $\boldsymbol{L}$ = 14 μm is the side length of the hexagonal microdisk. 9 WGMs can be clearly distinguished, with mode numbers $\boldsymbol{N_{TE}}$ calculated to be 452-481 according to their spectral peak positions. These resonant peaks located at 368.2, 370.5, 372.3, 374, 376.4, 379.5, 382.7, 386.1 and 389.4 nm are shown as the vertical dashed lines in Fig. 6(c) intersecting both the dispersion curve of the GaN (top) and the experimental lasing spectra (bottom). The theoretical resonance wavelengths of TE-modes are in good agreement with the experimentally measured spectrum of WGMs above lasing threshold, ambiguously demonstrating the TE-mode WGM lasing phenomenon [15,17,26].

Optics EXPRESS

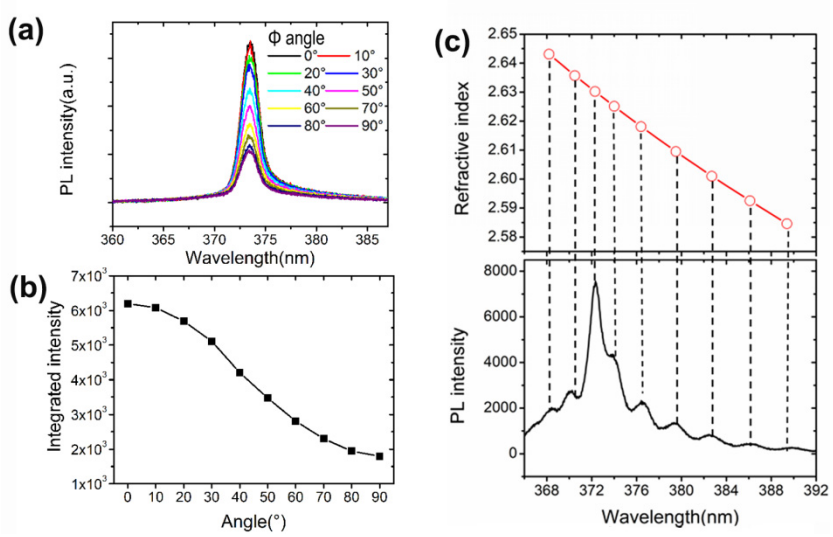

Fig. 6. Polarization dependent PL spectra of the 14 μm GaN microdisk, where TE (0°) and TM (90°) polarizations of the edge emissions were collected through a Glan-Talyor prism (a); Integrated PL intensity as a function of angle between polarizer prism and sample surface (b); Calculated resonant modes (dashed vertical lines) intersecting with the dispersion curve (top) and the experimental lasing spectrum (bottom) of the 14 μm GaN microdisk above lasing threshold (c).

Since GaN microdisk arrays were grown by SAG technique, high crystalline quality and thus better optical property at the overgrown region of the GaN microdisk are predicted, which is beneficial for WGM lasing as the resonant modes are localized along the edge of the microdisk. In order to demonstrate this hypothesis, bi-axial strain conditions were investigated. Micro-PL (μ-PL) mappings were generated from a 28 μm × 28 μm scanned area for a single 14 μm GaN microdisk. The spatial distribution of the emission wavelengths of a single 14 μm microdisk is extracted and rendered on Fig. 7(a). The average emission wavelength of the 14 μm GaN microdisk is around 362 nm. A red shift of approximately 0.5 nm from the center of the microdisk to the edge is clearly observed in Fig. 7(a), suggesting a change in the bi-axial strain condition. It is worth mentioning that the dominated lasing mode is approximately 372 nm. Therefore, the stimulated emission peak is located at the long-wavelength-side of the spontaneous emission peak, probably due to stronger re-absorption at the high-energy parts of the spontaneous emission spectrum, which is similar to our previous report for edge-emitting laser diode [19]. In order to qualitatively identify the strain relaxation process, spatially-resolved Raman spectroscopy was performed on the same GaN microdisk. Figure 7(b) shows the space distribution of the E_2 (high) position. Larger Raman shift is identified in the center region of the GaN microdisk compared to the edge. According to Tian *et al*., E_2 (high) position of a strain-free bulk GaN is located at 567.6 cm^{-1} at 300 K [27]. Therefore, compressive strain is identified in the center of the hexagonal GaN microdisk while strain relaxation occurs in the lateral overgrowth region of the microdisk due to the lateral overgrowth and thus lacking of lattice mismatch between GaN and sapphire substrate. The strain condition is consistent with the fact that the emission wavelength is red-shifted from the center to the edge of the GaN hexagonal microdisks [28]. The relaxation of compressive strain in the hexagonal GaN microdisk structure would result in the reduction of the piezoelectric field and improve the overlap of electron and hole wave functions, which greatly improves the radiative recombination rate in the GaN and benefits the stimulated emission and WGM lasing [29].

Optics EXPRESS

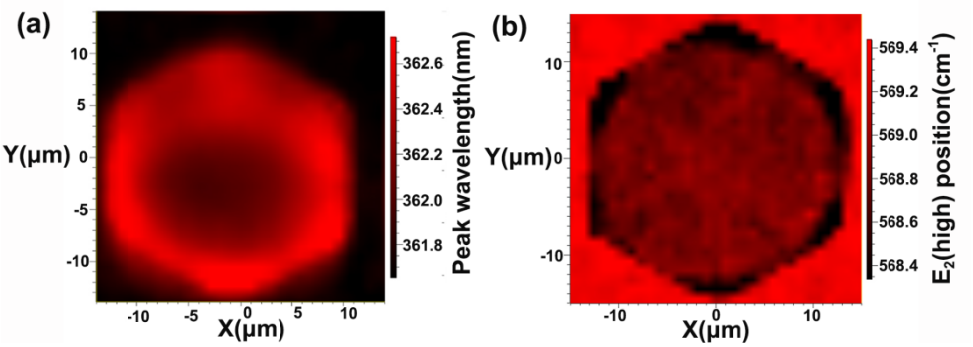

Fig. 7. Spatially-resolved PL mapping of the emission wavelength (a) and Raman spectroscopy of E_2 (high) peak position (b) of a single 14 μm GaN microdisk.

To provide a direct evidence on the relationship between crystalline quality and optical property of the GaN microdisk, RT CL measurement was carried out. Figure 8(a) shows the top view SEM image of the microdisk and Fig. 8(b) shows the spatially-resolved panchromatic CL intensity distribution of the GaN microdisk from 250 nm to 850 nm. Two dominant CL emission peaks at 370 nm and 550 nm are believed to be related to the near-band-edge (NBE) and deep-level emissions, as shown in (c) and (d), respectively. The defect-related yellow luminescence (YL) at around 550 nm has been observed by numerous researchers [30,31] and attributed to either carbon at nitrogen site C_N, or simply due to isolated V_{Ga}. The outlines of the SiO_2 microholes are denoted by the dashed red circles. Interestingly, NBE emissions originated mainly from the edge of the GaN microdisk, whereas the defect-related YL mostly came from the center region of the microdisk. The position-dependent CL luminescence indicated that the density of defect states associating with the nonradiative recombination centers are much lower in the laterally overgrown region than that in the center region of the GaN microdisk [17].

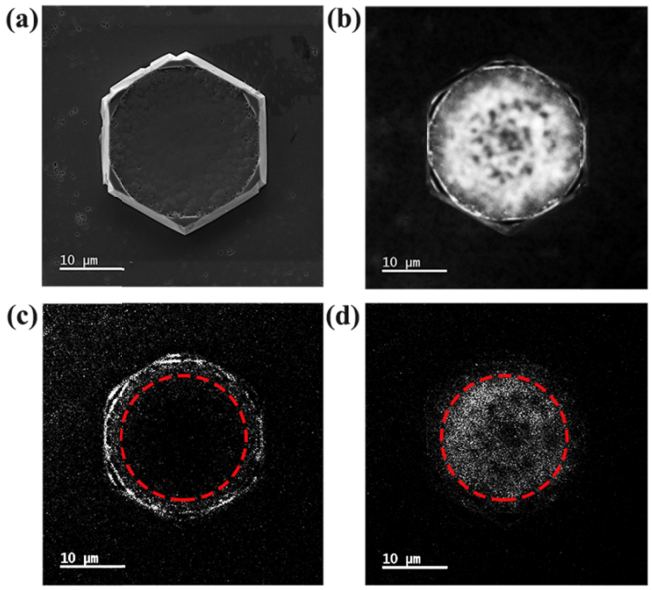

Fig. 8. Top-view SEM image (a) and CL intensity distribution of panchromatic (250-850 nm) (b), as well as monochromatic intensity distribution at λ = 370 nm (c) and λ = 550 nm (d) of the 14 μm GaN microdisk. The outlines of the underlying SiO_2 holes are denoted by the dashed red circles.

Optics EXPRESS

4. Conclusion

In summary, hexagonal GaN microdisks in a periodic array pattern were grown by SAG technique. WGM rather than F-P lasing is responsible for the observed stimulated emission. TE-dominant multimode lasing with a threshold of 2.43 MW/cm^2 and FWHM less than 2 nm are demonstrated from the 14 μm microdisk arrays at RT. Stimulated emissions are observed from various directions of the GaN microdisk, indicating the omnidirectional lasing behavior of the GaN microdisk due to various trajectories of the reflected light at the (0001) and (10-1-1) crystal planes. Furthermore, a relaxation of the compressive strain is confirmed by Raman spectroscopy, and it is consistent with the fact that PL emission wavelength is red-shifted from the center to the edge of the GaN hexagonal microdisk. CL luminescence suggests that the defect states are associated with the nonradiative recombination centers in the middle of the microdisk, whereas NBEs are mostly coming from the overgrown region of the GaN microdisk with better crystalline quality.

Funding

National Key Research and Development Program of China (Grant 2016YFB0400802), National Natural Science Foundation of China (Grants 61704176, 61574145, and 61874177), and Zhejiang Provincial Natural Science Foundation (Grant LY15F040003).

Acknowledgments

The authors appreciate the technical support from Nano Fabrication Facility, platform for Characterization & Test in Ningbo Institute of Materials Technology and Engineering, CAS.

References

1. R. Koester, J. S. Hwang, C. Durand, Dle. S. Dang, and J. Eymery, "Self-assembled growth of catalyst-free GaN wires by metal-organic vapour phase epitaxy," Nanotechnology **21**(1), 015602 (2010).
2. J. Méndez-Ramos, J. C. Ruiz-Morales, P. Acosta-Mora, and N. M. Khaidukov, "Infrared-light induced curing of photosensitive resins through photon up-conversion for novel cost-effective luminescent 3D-printing technology," J. Mater. Chem. C Mater. Opt. Electron. Devices **4**(4), 801–806 (2016).
3. M. Kushimoto, T. Tanikawa, Y. Honda, and H. Amano, "Optically pumped lasing properties of (1-101) InGaN/GaN stripe multiquantum wells with ridge cavity structure on patterned (001) Si substrates," Appl. Phys. Express **8**(2), 022702 (2015).
4. M. Feng, J. He, Q. Sun, H. Gao, Z. Li, Y. Zhou, J. Liu, S. Zhang, D. Li, L. Zhang, X. Sun, D. Li, H. Wang, M. Ikeda, R. Wang, and H. Yang, "Room-temperature electrically pumped InGaN-based microdisk laser grown on Si," Opt. Express **26**(4), 5043–5051 (2018).
5. H. Yoshida, Y. Yamashita, M. Kuwabara, and H. Kan, "A 342-nm ultraviolet AlGaN multiple-quantum-well laser diode," Nat. Photonics **2**(9), 551–554 (2008).
6. Y. Zhang, H. Li, P. Li, A. Dehzangi, L. Wang, X. Yi, and G. Wang, "Optically-Pumped Single-Mode Deep-Ultraviolet Microdisk Lasers With AlGaN-Based Multiple Quantum Wells on Si Substrate," IEEE Photonics J. **9**(5), 1–8 (2017).
7. Y. Sun, K. Zhou, Q. Sun, J. Liu, M. Feng, Z. Li, Y. Zhou, L. Zhang, D. Li, S. Zhang, M. Ikeda, S. Liu, and H. Yang, "Room-temperature continuous-wave electrically injected InGaN-based laser directly grown on Si," Nat. Photonics **10**(9), 595–599 (2016).
8. W. Guo, J. Li, M. Sheikhi, J. Jiang, Z. Yang, H. Li, S. Guo, J. Sheng, J. Sun, B. Bo, and J. Ye, "Comparative study on luminescence extraction strategies of LED by large-scale fabrication of nanopillar and nanohole structures," J. Phys. D Appl. Phys. **51**(24), 24LT01 (2018).
9. Y. T. Lin, T. W. Yeh, and P. D. Dapkus, "Mechanism of selective area growth of GaN nanorods by pulsed mode metalorganic chemical vapor deposition," Nanotechnology **23**(46), 465601 (2012).
10. S.-Y. Bae, K. Lekhal, H.-J. Lee, J.-W. Min, D.-S. Lee, Y. Honda, and H. Amano, "Selective-area growth of doped GaN nanorods by pulsed-mode MOCVD: Effect of Si and Mg dopants," Physica Status Solidi (b) **254**, 1600722 (2017).
11. J. R. Chang, S. P. Chang, Y. J. Li, Y. J. Cheng, K. P. Sou, J. K. Huang, H. C. Kuo, and C. Y. Chang, "Fabrication and luminescent properties of core-shell InGaN/GaN multiple quantum wells on GaN nanopillars," Appl. Phys. Lett. **100**(26), 261103 (2012).
12. C.-Y. Huang, T.-Y. Tai, J.-J. Lin, T.-C. Chang, C.-Y. Liu, T.-C. Lu, Y.-R. Wu, and H.-C. Kuo, "Mode-Hopping Phenomena in the InGaN-Based Core–Shell Nanorod Array Collective Lasing," ACS Photonics **5**(7), 2724–2729 (2018).
13. S. Mita, R. Collazo, and Z. Sitar, "Fabrication of a GaN lateral polarity junction by metalorganic chemical vapor

Optics EXPRESS

deposition," J. Cryst. Growth **311**(10), 3044–3048 (2009).
14. W. Guo, H. Sun, B. Torre, J. Li, M. Sheikhi, J. Jiang, H. Li, S. Guo, K.-H. Li, R. Lin, A. Giugni, E. Di Fabrizio, X. Li, and J. Ye, "Lateral-Polarity Structure of AlGaN Quantum Wells: A Promising Approach to Enhancing the Ultraviolet Luminescence," Adv. Funct. Mater. **28**(32), 1802395 (2018).
15. X. Zhang, Y. F. Cheung, Y. Zhang, and H. W. Choi, "Whispering-gallery mode lasing from optically free-standing InGaN microdisks," Opt. Lett. **39**(19), 5614–5617 (2014).
16. L. C. Wang, Y. Y. Zhang, R. Chen, Z. Q. Liu, J. Ma, Z. Li, X. Y. Yi, H. J. Li, J. X. Wang, G. H. Wang, W. H. Zhu, and J. M. Li, "Optically pumped lasing with a Q-factor exceeding 6000 from wet-etched GaN micro-pyramids," Opt. Lett. **42**(15), 2976–2979 (2017).
17. H. Baek, C. H. Lee, K. Chung, and G. C. Yi, "Epitaxial GaN microdisk lasers grown on graphene microdots," Nano Lett. **13**(6), 2782–2785 (2013).
18. H. W. Choi, P. T. Lai, and S. J. Chua, "Whispering-gallery mode lasing in GaN microdisks," in *SPIE*, 2007), 0692.
19. W. Guo, Z. Bryan, J. Xie, R. Kirste, S. Mita, I. Bryan, L. Hussey, M. Bobea, B. Haidet, M. Gerhold, R. Collazo, and Z. Sitar, "Stimulated emission and optical gain in AlGaN heterostructures grown on bulk AlN substrates," J. Appl. Phys. **115**(10), 103108 (2014).
20. H. Baek, J. K. Hyun, K. Chung, H. Oh, and G.-C. Yi, "Selective excitation of Fabry-Perot or whispering-gallery mode-type lasing in GaN microrods," Appl. Phys. Lett. **105**(20), 201108 (2014).
21. Z. Li, M. Jiang, Y. Sun, Z. Zhang, B. Li, H. Zhao, C. Shan, and D. Shen, "Electrically pumped Fabry-Perot microlasers from single Ga-doped ZnO microbelt based heterostructure diodes," Nanoscale **10**(39), 18774–18785 (2018).
22. G. Wang, X. Yi, L. Wang, P. Li, L. Liu, H. Li, and Y. Zhang, "UV-C whispering-gallery modes in AlN microdisks with AlGaN-based multiple quantum wells on Si substrate," J. Nanophotonics **12**, 1 (2018).
23. R. Chen, B. Ling, X. W. Sun, and H. D. Sun, "Room temperature excitonic whispering gallery mode lasing from high-quality hexagonal ZnO microdisks," Adv. Mater. **23**(19), 2199–2204 (2011).
24. K. Nam, J. Li, M. Nakarmi, J. Lin, and H. Jiang, "Unique optical properties of AlGaN alloys and related ultraviolet emitters," Appl. Phys. Lett. **84**(25), 5264–5266 (2004).
25. C. Tessarek, G. Sarau, M. Kiometzis, and S. Christiansen, "High quality factor whispering gallery modes from self-assembled hexagonal GaN rods grown by metal-organic vapor phase epitaxy," Opt. Express **21**(3), 2733–2740 (2013).
26. T. Kouno, K. Kishino, and M. Sakai, "Lasing Action on Whispering Gallery Mode of Self-Organized GaN Hexagonal Microdisk Crystal Fabricated by RF-Plasma-Assisted Molecular Beam Epitaxy," IEEE J. Quantum Electron. **47**(12), 1565–1570 (2011).
27. W. Tian, W. Y. Yan, X. Hui, S. L. Li, Y. Y. Ding, Y. Li, Y. Tian, J. N. Dai, Y. Y. Fang, Z. H. Wu, C. H. Yu, and C. Q. Chen, "Tunability of intersubband transition wavelength in the atmospheric window in AlGaN/GaN multi-quantum wells grown on different AlGaN templates by metalorganic chemical vapor deposition," J. Appl. Phys. **112**(6), 063526 (2012).
28. J. Mickevičius, T. Grinys, A. Kadys, and G. Tamulaitis, "Optimization of growing green-emitting InGaN/GaN multiple quantum wells on stress-relieving superlattices," Opt. Mater. **82**, 71–74 (2018).
29. W. Tawfik, J. Song, J. J. Lee, J. S. Ha, S.-W. Ryu, H. S. Choi, B. Ryu, and J. K. Lee, "Effect of external tensile stress on blue InGaN/GaN multi-quantum-well light-emitting diodes," Appl. Surf. Sci. **283**(14), 727–731 (2013).
30. Q. Li and G. T. Wang, "Spatial distribution of defect luminescence in GaN nanowires," Nano Lett. **10**(5), 1554–1558 (2010).
31. P. Reddy, M. P. Hoffmann, F. Kaess, Z. Bryan, I. Bryan, M. Bobea, A. Klump, J. Tweedie, R. Kirste, S. Mita, M. Gerhold, R. Collazo, and Z. Sitar, "Point defect reduction in wide bandgap semiconductors by defect quasi Fermi level control," J. Appl. Phys. **120**(18), 185704 (2016).